applied sciences

MDPI

Article

SH Wave Scattering and Dynamic Stress Concentration in Piezomagnetic Materials with Non-Circular Openings

Chuanping Zhou, Jiayou Weng *, Zhiwen Wang *, Wanrong Pei *, Ning Hu, Rougang Zhou and Youping Gong

School of Mechanical Engineering, Hangzhou Dianzi University, Hangzhou 310018, China; zhoucp@hdu.edu.cn (C.Z.); hooning@hdu.edu.cn (N.H.); 42141@hdu.edu.cn (R.Z.); gyp@hdu.edu.cn (Y.G.)
* Correspondence: joany0204@163.com (J.W.); wzw3049972460@hdu.edu.cn (Z.W.); wrpei@hdu.edu.cn (W.P.)

Abstract: The study uses complex variable functions and conformal mapping to investigate the scattering and dynamic stress concentration phenomena of SH waves in non-circular opening magnetic–elastic materials. Elastic dynamics and piezomagnetic equations are employed to derive expressions for the scattered wave intensity and dynamic stress concentration coefficient around non-circular openings. Special attention is devoted to elliptical openings, where different incident angles and dimensionless wave numbers exhibit varying effects on the dynamic stress concentration coefficients. The numerical results indicate a positive correlation between the dynamic stress concentration coefficient and the illumination region of elliptical openings, with low wave numbers exerting a more significant influence. These findings provide a valuable theoretical foundation for studying fatigue mechanics in piezomagnetic materials. Therefore, to enhance the performance and reliability of piezomagnetic materials, it is imperative to conduct elastic dynamic analysis of non-circular defects in low-frequency environments.

Keywords: piezomagnetic materials; SH wave; dynamic stress concentration coefficient; conformal mapping; non-circular opening

check for updates

Citation: Zhou, C.; Weng, J.; Wang, Z.; Pei, W.; Hu, N.; Zhou, R.; Gong, Y. SH Wave Scattering and Dynamic Stress Concentration in Piezomagnetic Materials with Non-Circular Openings. *Appl. Sci.* **2023**, *13*, 6972. https://doi.org/10.3390/app13126972

Academic Editor: Luigi La Spada

Received: 21 May 2023
Revised: 4 June 2023
Accepted: 5 June 2023
Published: 9 June 2023

Copyright: © 2023 by the authors. Licensee MDPI, Basel, Switzerland. This article is an open access article distributed under the terms and conditions of the Creative Commons Attribution (CC BY) license (https://creativecommons.org/licenses/by/4.0/).

1. Introduction

Piezomagnetic materials are functional materials that exhibit magnetic deformation when subjected to an external magnetic field. These materials find extensive applications in manufacturing non-invertible or invertible devices, including isolation devices, oscillators, filters, circulators, and modulators, as well as in fields, such as radar and satellite communication. Piezomagnetic materials used to produce high-precision intelligent components have become a rapidly developing and widely used field. However, during the processing and utilization of these materials, issues such as stress concentration due to defects (such as pores, cracks, and composite forms) can significantly reduce the expected lifespan and cause the materials to lose their original design functionality, leading to medium breakdown or failure. Therefore, the academic community has devoted considerable attention to addressing the reliability and stability issues of piezomagnetic materials [1,2].

The academic community is actively engaged in research to enhance the performance and reliability of piezomagnetic materials, which involves detecting and analyzing defects in these materials and the study of stress concentration and fracture mechanisms associated with these defects. Soh et al. [3] investigated the conditions for surface harmonic waves (SH waves) at the interface between adhesive half-infinite piezoelectric and magnetic materials. They discovered that SH waves are generated and propagated at the interface of the material film within a specific frequency range, provided that the interface stiffness satisfies certain conditions. On the other hand, Singh et al. [4] researched the propagation behavior of SH waves at the interface of adhesive infinite piezoelectric and magnetic materials. Both of these studies focused on functional gradient materials, where changes in material parameters occurred along directions parallel and perpendicular to the interface.

Considering the influence of imperfect interfaces, Wei et al. [5] investigated the diffraction problem of surface harmonic waves (SH waves) in piezoelectric/piezomagnetic plates. They demonstrated the effectiveness of the numerical solution process by solving the diffraction equation and verifying its validity through analytical derivation. Similarly, Huang et al. [6] studied the diffraction relationship of SH waves propagating along an imperfect interface in magnetic/piezoelectric composite materials. They discovered that interface SH waves only exist at poor interfaces in specific magnetic/piezoelectric composite material combinations. These studies have significant implications for further understanding the propagation rules of SH waves in materials.

Nie et al. [7] investigated the propagation of SH waves in a double-layer system consisting of piezoelectric and magnetic layers. They provide numerical examples to illustrate the effects of electromagnetic boundary conditions, imperfect interfaces, different piezoelectric layers, and thickness ratios on diffraction behavior. Kuo et al. [8] performed a detailed analysis of the scattering behavior of SH waves from piezoelectric cylinders in a piezoelectric–electromagnetic matrix with imperfect interfaces. They studied two typical discontinuous interfaces to obtain the impact of scattering cross-section and field distribution. Additionally, Sun et al. [9] studied the propagation of SH waves in ferromagnetic multiferroic composite materials composed of piezoelectric layers and magnetic central cylinders. They obtained the diffraction relationship of SH waves under two different electromagnetic boundary conditions. Liu et al. explored the propagation of SH waves in periodically layered magnetic structures and derived the diffraction equation and transmission coefficient. This study revealed the wave behavior of SH waves when the magnetic path is closed or opened, providing important implications for understanding the propagation rules and applications of SH waves in periodically structured systems. On the other hand, Qian et al. [10] studied the propagation of SH waves in occasionally layered piezoelectric materials based on a perfect alternate structure of piezoelectric films and polymer films. They obtained the phase velocity equation, discussing the filtering effect of this structure and the impact of volume fraction and shear modulus ratio of piezoelectric layers and polymer layers on the phase velocity. This study provides important insights for designing new piezoelectric phonon crystal devices. Wang et al. [11] studied the propagation of elastic waves in a phonon crystal containing piezoelectric and magnetic encapsulation bodies based on magnetic–electric elastic coupling while regarding the electric and magnetic fields as quasi-static. Their research has significant value for piezoelectric/piezomagnetic composite materials in microwave technology, promoting a deeper understanding of the properties of this composite material and its applications in related fields.

Electromagnetic composite materials have multiple properties that have received extensive attention in electromagnetic fields. In recent decades, many scholars have dedicated themselves to studying electromagnetic composite materials' mechanical and electrical properties. For example, Liu et al. [12] studied the problem of an infinite two-dimensional anisotropic piezoelectric–piezomagnetic medium containing elliptical pores. Subsequently, Pan et al. [13] extended this method to the free vibration problem of an infinite-length anisotropic-supported piezoelectric–piezomagnetic laminate and provided numerical examples for a single-layer piezoelectric plate, a two-layer piezoelectric–piezomagnetic laminate, and a four-layer piezoelectric–piezomagnetic laminate. Pan et al. [14] solved the problem of a three-dimensional anisotropic functional gradient piezoelectric–piezomagnetic rectangular laminate under the combined action of mechanical and electrical loads. They applied the variational principle to transform the problem of combined mechanical and electrical loads into an individual load problem. These research results provide necessary theoretical support for applying electromagnetic composite materials.

In elastic dynamics, various mathematical methods are employed to study the propagation of SH waves. Pang et al. [15] utilized the stiffness matrix method and the transmission matrix method to investigate the transmission of SH waves through infinite/semi-infinite piezoelectric/piezoelectric and periodic composite materials. Ezzin et al. [16]

studied the propagation of SH waves through piezoelectric/piezomagnetic plates using constant differential equations and the stiffness matrix method. They discussed the impact of film thickness on the phase, group, and first-mode magnetic–mechanical coupling factor. Nobili et al. [17] employed the coupled stress elastic indeterminacy theory to investigate the mechanical behavior of materials. They obtained the global solution for crack problems through integral transformation and the Wiener–Hopf technique. Wang et al. [18] used complex and potential functions to study the scattering of plane harmonic waves via multiple elliptical cavities in a water-saturated soil medium. Yu et al. [19] proposed a double orthogonal polynomial series method, which can be used to design and optimize multi-layer piezoelectric voltage–magnetic material transducers.

Lamb waves and surface waves hold great importance in research as unique waves. Cao et al. [20] studied the propagation of Lamb waves in a functional gradient piezoelectric–piezomagnetic material plate, considering the continuous change in material parameters along the thickness direction. They solved the constant differential equation with variable coefficients using the power series method and considered the continuous variation in material parameters along the thickness direction. Pang et al. [21] calculated the dispersion curves and displacement fields of Lamb waves in layer-periodic composite materials composed of piezoelectric–piezomagnetic materials for different volume fractions of piezoelectric materials. Li et al. [22] used the Bond transformation to study the impact of piezoelectric and magnetic effects on the surface wave velocity of magnetic elastic solids. They derived the long-term equation satisfied by the surface wave velocity. Zakharovenko et al. [23] studied the characteristics of shear-horizontal surface acoustic waves in Alfenol, Terfenol-D, Metglas, and $NiFe_2O_4$ piezoelectric cubic single crystals. These research results provide theoretical guidance for analyzing and designing magnetic and electric transducers in functional gradient materials and provide academic advice for ultrasound non-destructive evaluation. Additionally, piezoelectric–piezomagnetic materials have extensive applications in biomedical engineering, such as ultrasound imaging and treatment.

In summary, scholars have extensively researched the elastic dynamics and structural dynamics of piezoelectric materials and their composite materials. However, research on the structural dynamic behavior of non-circular open magnetic materials is relatively rare. Given the widespread application of piezoelectric and magnetic materials, studying the dynamic stress concentration is of great value.

2. Governing Equations

For a steady-state elastic field and electric field under the action of a periodic load, the field variables can be expressed in the following separated form with time-harmonic factors and spatial variables

$$L^*(x, y, t) = L(x, y)\mathrm{e}^{-\mathrm{i}\omega t}, \tag{1}$$

where L^* is a complex function and its real part is the solution of the problem. The spatial function L is the main subject of study.

Considering the case of SH wave incident on the xy-plane, assuming that the z-axis is the polarization direction, the control equations of the steady-state anti-plane dynamic problem are

$$\begin{aligned} &\frac{\partial \tau_{xz}}{\partial x} + \frac{\partial \tau_{yz}}{\partial y} + \rho\omega^2 w = 0, \\ &\frac{\partial B_x}{\partial x} + \frac{\partial B_y}{\partial y} = 0, \end{aligned} \tag{2}$$

where the components τ_{xz} and τ_{yz} are the anti-plane shear stress components; B_x and B_y are the magnetic displacement components. w, ρ, and ω, respectively, represent the displacement on the z-axis, the density, and the circular frequency of the steady-state waves.

Thus, the constitutive relation of piezomagnetic materials can be expressed as

$$\begin{array}{l} \tau_{xz} = c_{44}\frac{\partial w}{\partial x} + h_{15}\frac{\partial \phi}{\partial x}, \tau_{yz} = c_{44}\frac{\partial w}{\partial y} + h_{15}\frac{\partial \phi}{\partial y}, \\ B_x = h_{15}\frac{\partial w}{\partial x} - \mu_{11}\frac{\partial \phi}{\partial x}, B_y = h_{15}\frac{\partial w}{\partial y} - \mu_{11}\frac{\partial \phi}{\partial y}, \end{array} \tag{3}$$

where the c_{44}, $h_{15,}$ and μ_{11} represent the elastic constants, piezomagnetic stress constants, and magnetic constants, respectively. ϕ represents the magnetic potential within the medium.

Substituting Equation (3) into Equation (2), we can obtain the following form

$$\begin{array}{l} \nabla^2 w + k^2 w = 0, \\ \nabla^2 f = 0, \end{array} \tag{4}$$

where the $k = \sqrt{\rho\omega^2/c^*}$ represents the wave number and $c^* = c_{44} + h_{15}^2/\mu_{11}$ represents the modulus of magnetic hardening elastic constant.

The magnetic potential can be determined by

$$\phi = \frac{h_{15}}{\mu_{11}}(w + f). \tag{5}$$

In a cylindrical coordinate system, Equation (4) can be written in the following form

$$\begin{array}{l} \frac{\partial^2 w}{\partial r^2} + \frac{1}{r}\frac{\partial w}{\partial r} + \frac{1}{r^2}\frac{\partial^2 w}{\partial \alpha^2} + k^2 w = 0, \\ \frac{\partial^2 f}{\partial r^2} + \frac{1}{r}\frac{\partial f}{\partial r} + \frac{1}{r^2}\frac{\partial^2 f}{\partial \alpha^2} = 0. \end{array} \tag{6}$$

Meanwhile, Equation (3) can be transformed into the following form

$$\begin{array}{l} \tau_{rz} = c_{44}\frac{\partial w}{\partial r} + h_{15}\frac{\partial \phi}{\partial r}, \tau_{\alpha z} = c_{44}\frac{1}{r}\frac{\partial w}{\partial \alpha} + h_{15}\frac{1}{r}\frac{\partial \phi}{\partial \alpha}, \\ B_r = h_{15}\frac{\partial w}{\partial r} - \mu_{11}\frac{\partial \phi}{\partial r}, B_\alpha = h_{15}\frac{1}{r}\frac{\partial w}{\partial \alpha} - \mu_{11}\frac{1}{r}\frac{\partial \phi}{\partial \alpha}. \end{array} \tag{7}$$

The method of complex function and conformal mapping can be employed to solve the boundary value problem of non-circular openings, as shown in Figure 1. After introducing complex variables $z = re^{i\alpha}$ and $\overline{z} = re^{-i\alpha}$ and using conformal mapping, Equation (4) can be expressed as

$$\begin{array}{l} \frac{\partial^2 w}{\partial \zeta \partial \overline{\zeta}} = \left(\frac{ik}{2}\right)^2 \hbar'(\zeta)\overline{\hbar'(\zeta)}w(\zeta, \overline{\zeta}), \\ \frac{\partial^2 f}{\partial \zeta \partial \overline{\zeta}} = 0. \end{array} \tag{8}$$

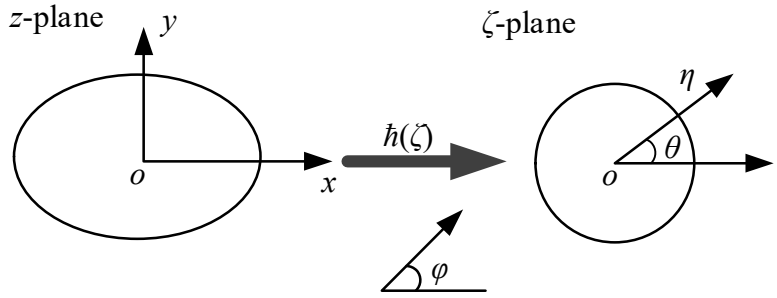


Figure 1. The outer domain of the non-circular boundary of the z-plane is mapped to the outer domain of the unit circle of the ζ-plane.

On the mapping plane (η, θ), we can utilize the following equation

$$\left\{ \begin{array}{l} \frac{\partial}{\partial r} = \frac{\partial}{\partial z}e^{i\alpha} + \frac{\partial}{\partial \overline{z}}e^{-i\alpha} \\ \frac{\partial}{\partial \alpha} = iz\frac{\partial}{\partial z} - i\overline{z}\frac{\partial}{\partial \overline{z}} \end{array} \right., e^{i\alpha} = \frac{\hbar'(\zeta)}{|\hbar'(\zeta)|}e^{i\theta}, dz = \hbar'(\zeta)d\zeta. \tag{9}$$

Equation (7) can be transformed as

$$\begin{aligned}
\tau_{\eta z} &= \frac{c^*}{\left|\hbar'(\zeta)\right|}\left(\frac{\partial w}{\partial \zeta}\mathrm{e}^{\mathrm{i}\theta} + \frac{\partial w}{\partial \overline{\zeta}}\mathrm{e}^{-\mathrm{i}\theta}\right) + \frac{h_{15}^2/\mu_{11}}{\left|\hbar'(\zeta)\right|}\left(\frac{\partial f}{\partial \zeta}\mathrm{e}^{\mathrm{i}\theta} + \frac{\partial f}{\partial \overline{\zeta}}\mathrm{e}^{-\mathrm{i}\theta}\right),\\
\tau_{\theta z} &= \frac{\mathrm{i}c^*}{\left|\hbar'(\zeta)\right|}\left(\frac{\partial w}{\partial \zeta}\mathrm{e}^{\mathrm{i}\theta} - \frac{\partial w}{\partial \overline{\zeta}}\mathrm{e}^{-\mathrm{i}\theta}\right) + \frac{\mathrm{i}h_{15}^2/\mu_{11}}{\left|\hbar'(\zeta)\right|}\left(\frac{\partial f}{\partial \zeta}\mathrm{e}^{\mathrm{i}\theta} - \frac{\partial f}{\partial \overline{\zeta}}\mathrm{e}^{-\mathrm{i}\theta}\right),\\
B_\eta &= -\frac{h_{15}}{\left|\hbar'(\zeta)\right|}\left(\frac{\partial f}{\partial \zeta}\mathrm{e}^{\mathrm{i}\theta} + \frac{\partial f}{\partial \overline{\zeta}}\mathrm{e}^{-\mathrm{i}\theta}\right),\\
B_\theta &= -\frac{\mathrm{i}h_{15}}{\left|\hbar'(\zeta)\right|}\left(\frac{\partial f}{\partial \zeta}\mathrm{e}^{\mathrm{i}\theta} - \frac{\partial f}{\partial \overline{\zeta}}\mathrm{e}^{-\mathrm{i}\theta}\right).
\end{aligned} \tag{10}$$

In the original plane, the angle between the SH wave vector and the positive x-axis vector is denoted as φ. In the mapping plane, we can express the elastic field and magnetic potential as follows

$$\begin{aligned}
w^{(i)} &= w_0\mathrm{e}^{\frac{\mathrm{i}k}{2}[\hbar(\zeta)\mathrm{e}^{-\mathrm{i}\varphi}+\overline{\hbar(\zeta)}\mathrm{e}^{\mathrm{i}\varphi}]},\\
\phi^{(i)} &= \frac{h_{15}}{\mu_{11}}w_0\mathrm{e}^{\frac{\mathrm{i}k}{2}[\hbar(\zeta)\mathrm{e}^{-\mathrm{i}\varphi}+\overline{\hbar(\zeta)}\mathrm{e}^{\mathrm{i}\varphi}]},
\end{aligned} \tag{11}$$

where the w_0 is the amplitude of the incident wave. The above equation omits the time factor $\mathrm{e}^{-\mathrm{i}\omega t}$.

By employing the wave function expansion method, we can express Equation (11) as follows

$$\begin{aligned}
w^{(i)} &= w_0\sum_{n=-\infty}^{\infty}\mathrm{i}^n J_n(k|\hbar(\zeta)|)\left\{\frac{\hbar(\zeta)}{|\hbar(\zeta)|}\right\}^n\mathrm{e}^{-\mathrm{i}n\varphi},\\
\phi^{(i)} &= \frac{h_{15}}{\mu_{11}}w_0\sum_{n=-\infty}^{\infty}\mathrm{i}^n J_n(k|\hbar(\zeta)|)\left\{\frac{\hbar(\zeta)}{|\hbar(\zeta)|}\right\}^n\mathrm{e}^{-\mathrm{i}n\varphi}.
\end{aligned} \tag{12}$$

Simultaneously, the scattered wave generated by an irregular opening can be expressed as

$$\begin{aligned}
w^{(s)} &= w_0\sum_{n=-\infty}^{\infty}A_n H_n^{(1)}(k|\hbar(\zeta)|)\left\{\frac{\hbar(\zeta)}{|\hbar(\zeta)|}\right\}^n,\\
f^{(s)} &= B_0 + w_0\sum_{n=1}^{\infty}\left(B_n\zeta^{-n} + C_n\overline{\zeta}^{-n}\right),\\
\phi^{(s)} &= \frac{h_{15}}{\mu_{11}}\left(w^{(s)} + f^{(s)}\right),
\end{aligned} \tag{13}$$

where the $H_n^{(1)}$ represents the first-type Hankle function, and A_n, B_n, C_n, and B_0 are undetermined constants.

For piezomagnetic materials, we can express the total elastic field and total magnetic potential as follows

$$\begin{aligned}
w^{(t)} &= w_0\sum_{n=-\infty}^{\infty}\left[\mathrm{i}^n J_n(k|\hbar(\zeta)|)\mathrm{e}^{-\mathrm{i}n\varphi} + A_n H_n^{(1)}(k|\hbar(\zeta)|)\right]\left\{\frac{\hbar(\zeta)}{|\hbar(\zeta)|}\right\}^n,\\
f^{(t)} &= B_0 + w_0\sum_{n=1}^{\infty}\left(B_n\zeta^{-n} + C_n\overline{\zeta}^{-n}\right),\\
\phi^{(t)} &= \frac{h_{15}}{\mu_{11}}\left(w^{(t)} + f^{(t)}\right).
\end{aligned} \tag{14}$$

Consider condition $|\zeta| \to \infty$, $\phi^{(t)} \to \phi^{(i)}$, $B_0 = 0$ can be obtained.

We can express the magnetic potential of the opening with no elastic field but a magnetic field $\nabla^2\phi^{(I)} = 0$ as follows

$$\phi^{(I)} = \frac{h_{15}}{\mu_{11}}w_0\left[D_0 + \sum_{n=1}^{\infty}\left(D_n\zeta^n + E_n\overline{\zeta}^n\right)\right], \tag{15}$$

where D_n, E_n, and D_0 are undetermined constants.

3. Boundary Conditions and Modal Coefficients

On the mapping plane, we can represent the boundary conditions as follows

$$\tau_{\eta z}^{(t)}\Big|_{\zeta_0} = 0,\ B_{\eta}^{(t)}\Big|_{\zeta_0} = B_{\eta}^{(I)}\Big|_{\zeta_0},\ \phi^{(t)}\Big|_{\zeta_0} = \phi^{(I)}\Big|_{\zeta_0}. \tag{16}$$

By utilizing Equation (5) and substituting the third equation of Equation (10) into the second equation of Equation (16), we can obtain

$$h_{15}\left(\frac{\partial f^{(t)}}{\partial \zeta}\mathrm{e}^{\mathrm{i}\theta} + \frac{\partial f^{(t)}}{\partial \overline{\zeta}}\mathrm{e}^{-\mathrm{i}\theta}\right) = \mu_0\left(\frac{\partial \phi^{(I)}}{\partial \zeta}\mathrm{e}^{\mathrm{i}\theta} + \frac{\partial \phi^{(I)}}{\partial \overline{\zeta}}\mathrm{e}^{-\mathrm{i}\theta}\right). \tag{17}$$

where μ_0 is the vacuum permeability.

By utilizing the second formula of Equations (14) and (15), we can express Equation (17) as follows

$$-\mu_{11}\sum_{n=1}^{\infty} n\left(B_n\zeta^{-n-1}\mathrm{e}^{\mathrm{i}\theta} + C_n\overline{\zeta}^{-n-1}\mathrm{e}^{-\mathrm{i}\theta}\right) = \mu_0\sum_{n=1}^{\infty} n\left(D_n\zeta^{n-1}\mathrm{e}^{\mathrm{i}\theta} + E_n\overline{\zeta}^{n-1}\mathrm{e}^{-\mathrm{i}\theta}\right). \tag{18}$$

Assuming that the mapping plane of the opening is the unit circle, we can express Equations $\zeta = \eta\mathrm{e}^{\mathrm{i}\theta}$ and $\eta = 1$, as well as Equation (18), as follows

$$\sum_{n=1}^{\infty} n\left[\left(\frac{\mu_{11}}{\mu_0}B_n + D_n\right)\mathrm{e}^{-\mathrm{i}n\theta} + \left(\frac{\mu_{11}}{\mu_0}C_n + E_n\right)\mathrm{e}^{\mathrm{i}n\theta}\right] = 0. \tag{19}$$

As $\mathrm{e}^{-\mathrm{i}n\theta}$ and $\mathrm{e}^{\mathrm{i}n\theta}$ are both non-zero and independent of each other, we can conclude that

$$\begin{cases} D_n = -\frac{\mu_{11}}{\mu_0}B_n \\ E_n = -\frac{\mu_{11}}{\mu_0}C_n \end{cases}, n \geq 1. \tag{20}$$

By substituting the third equation of Equations (14), (15), and (20) into the third equation of Equation (16), we obtain

$$\begin{aligned} 0 = &\sum_{n=-\infty}^{\infty}\left[\mathrm{i}^n J_n(k|\hbar(\zeta)|)\mathrm{e}^{-\mathrm{i}n\varphi} + A_n H_n^{(1)}(k|\hbar(\zeta)|)\right]\left\{\frac{\hbar(\zeta)}{|\hbar(\zeta)|}\right\}^n \\ &+\left(1+\tfrac{\mu_{11}}{\mu_0}\right)\sum_{n=1}^{\infty}\left(B_n\mathrm{e}^{-\mathrm{i}n\theta} + C_n\mathrm{e}^{\mathrm{i}n\theta}\right) - D_0. \end{aligned} \tag{21}$$

Substituting the first equation of Equation (10) into the first equation of Equation (16), we obtain

$$\frac{c^*}{|\hbar'(\zeta)|}\left(\frac{\partial w^{(t)}}{\partial \zeta}\mathrm{e}^{\mathrm{i}\theta} + \frac{\partial w^{(t)}}{\partial \overline{\zeta}}\mathrm{e}^{-\mathrm{i}\theta}\right) + \frac{h_{15}^2/\mu_{11}}{|\hbar'(\zeta)|}\left(\frac{\partial f^{(t)}}{\partial \zeta}\mathrm{e}^{\mathrm{i}\theta} + \frac{\partial f^{(t)}}{\partial \overline{\zeta}}\mathrm{e}^{-\mathrm{i}\theta}\right) = 0. \tag{22}$$

We can obtain the following relation

$$\begin{aligned} \frac{\partial}{\partial \overline{\zeta}}\left[H_n(k|\hbar(\zeta)|)\left\{\frac{\hbar(\zeta)}{|\hbar(\zeta)|}\right\}^n\right] &= \tfrac{k}{2}H_{n-1}(k|\hbar(\zeta)|)\left\{\frac{\hbar(\zeta)}{|\hbar(\zeta)|}\right\}^{n-1}\hbar'(\zeta), \\ \frac{\partial}{\partial \overline{\zeta}}\left[H_n(k|\hbar(\zeta)|)\left\{\frac{\hbar(\zeta)}{|\hbar(\zeta)|}\right\}^n\right] &= -\tfrac{k}{2}H_{n+1}(k|\hbar(\zeta)|)\left\{\frac{\hbar(\zeta)}{|\hbar(\zeta)|}\right\}^{n+1}\overline{\hbar'(\zeta)}. \end{aligned} \tag{23}$$

By utilizing Equation (23), Equation (22) can be expressed as follows

$$\begin{aligned} 0 = {} & k\sum_{n=-\infty}^{\infty}\left[\mathrm{i}^n\mathrm{e}^{-\mathrm{i}n\varphi}J_{n-1}(k|\hbar(\zeta)|)+A_nH_{n-1}^{(1)}(k|\hbar(\zeta)|)\right]\left\{\frac{\hbar(\zeta)}{|\hbar(\zeta)|}\right\}^{n-1}\hbar'(\zeta)\mathrm{e}^{\mathrm{i}\theta} \\ & -k\sum_{n=-\infty}^{\infty}\left[\mathrm{i}^n\mathrm{e}^{-\mathrm{i}n\varphi}J_{n+1}(k|\hbar(\zeta)|)+A_nH_{n+1}^{(1)}(k|\hbar(\zeta)|)\right]\left\{\frac{\hbar(\zeta)}{|\hbar(\zeta)|}\right\}^{n+1}\overline{\hbar'(\zeta)}\mathrm{e}^{-\mathrm{i}\theta} \\ & +\tfrac{2\lambda}{1+\lambda}\sum_{n=1}^{\infty}n\left(B_n\mathrm{e}^{-\mathrm{i}n\theta}+C_n\mathrm{e}^{\mathrm{i}n\theta}\right), \end{aligned} \tag{24}$$

where $\lambda = h_{15}^2/c_{44}\mu_{11}$ is a dimensionless parameter that characterizes the fundamental properties of piezomagnetic materials.

By multiplying both sides of Equations (21) and (24) by $\mathrm{e}^{-\mathrm{i}m\theta}$ ($\mathrm{m} \in \boldsymbol{Z}$) and integrating over interval (0, 2π), we can obtain an infinite system of algebraic equations in the following form

$$\sum_{n=-\infty}^{\infty}F_{in}A_n+\sum_{n=1}^{\infty}I_{in}B_n+\sum_{n=1}^{\infty}P_{in}C_n+Q_iD_0=\varepsilon_i, \tag{25}$$

where the elements F_{in}, I_{in}, P_{in}, Q_i, and ε_i in the equation are listed in Appendix A.

As cylindrical functions exhibit convergence, we can set n as the maximum value of N in Equation (25), i.e., $n = N$. This results in $2N + 1$ undetermined coefficients for A_n, N undetermined coefficients for B_n and C_n, and one undetermined coefficient for D_0, making a total of $4N + 2$ undetermined coefficients. With two infinite algebraic equations, we can construct $4N + 2$ equations, providing sufficient conditions to solve these undetermined coefficients. To solve the equation $\boldsymbol{\Omega X} = \boldsymbol{\Psi}$, where $\boldsymbol{X}$ is a $(4N + 2) \times 1$ order matrix of undetermined coefficients, we employ linear algebra theory. $\boldsymbol{\Omega}$ is a square matrix of order $(4N + 2) \times (4N + 4)$, constructed by F_{1n}, F_{2n}, I_{1n}, I_{2n}, P_{1n}, P_{2n}, Q_1, and Q_2, serving as the coefficient matrix. Meanwhile, $\boldsymbol{\Psi}$ is a non-homogeneous coefficient matrix, which is a $(4N + 2) \times 1$ matrix constructed by ε_1 and ε_2. We then use $\boldsymbol{X} = \boldsymbol{\Omega}^{-1}\boldsymbol{\Psi}$ to obtain the solution for the undetermined coefficients.

4. Dynamic Stress Concentration Coefficient around Elliptical Opening

By substituting Equation (14) into Equation (10) using Equation (23), we obtain Equation (2), which indicates that the stress exerted around the opening is

$$\begin{aligned} \tau_{\theta z}^{t} = c_{44}w_0k\Bigg\{ & -\lambda\sum_{n=1}^{\infty}\left(B_n\mathrm{e}^{-\mathrm{i}n\theta}+C_n\mathrm{e}^{\mathrm{i}n\theta}\right)\frac{n}{k\left|\hbar'(\zeta)\right|} \\ & +(1+\lambda)\sum_{n=-\infty}^{\infty}\left[\mathrm{i}^n\mathrm{e}^{-\mathrm{i}n\varphi}J_{n-1}(k|\hbar(\zeta)|)+A_nH_{n-1}^{(1)}(k|\hbar(\zeta)|)\right]\left\{\frac{\hbar(\zeta)}{|\hbar(\zeta)|}\right\}^{n-1}\frac{\hbar'(\zeta)\mathrm{e}^{\mathrm{i}\theta}}{2\left|\hbar'(\zeta)\right|} \\ & +(1+\lambda)\sum_{n=-\infty}^{\infty}\left[\mathrm{i}^n\mathrm{e}^{-\mathrm{i}n\varphi}J_{n+1}(k|\hbar(\zeta)|)+A_nH_{n+1}^{(1)}(k|\hbar(\zeta)|)\right]\left\{\frac{\hbar(\zeta)}{|\hbar(\zeta)|}\right\}^{n+1}\frac{\overline{\hbar'(\zeta)}\mathrm{e}^{-\mathrm{i}\theta}}{2\left|\hbar'(\zeta)\right|}\Bigg\}. \end{aligned} \tag{26}$$

The definition of the dynamic stress concentration coefficient (DSCC) around the opening is as follows

$$DSCC = \left|\tau_{\theta z}^{t}/\tau_0\right|, \tag{27}$$

where the physical significance of $\tau_0 = c_{44}kw_0$ is the stress amplitude produced by an SH wave incident on the material without any defect.

The elliptical opening is a unique form of non-circular opening, and its solution necessitates the derivation of an appropriate mapping function. The theory of conformal mapping provides a means to obtain this mapping function, which is given by

$$\hbar(\zeta) = \frac{a+b}{2}\zeta+\frac{a-b}{2\zeta}, \tag{28}$$

where a and b denote the length of the major and minor semi-axes of the ellipse, respectively. The region outside the elliptical opening in the original plane is mapped to the region surrounding the circular opening in the mapping plane.

The derivative of Equation (28) can be expressed as

$$\hbar'(\zeta) = \frac{a+b}{2} - \frac{a-b}{2}\frac{1}{\zeta^2}. \tag{29}$$

When $\zeta = e^{i\theta}$, Equations (28) and (29) can be expressed as

$$\begin{array}{l} \hbar(\theta) = \frac{a+b}{2}e^{i\theta} + \frac{a-b}{2}e^{-i\theta}, \\ \hbar'(\theta) = \frac{a+b}{2} - \frac{a-b}{2}e^{-2i\theta}. \end{array} \tag{30}$$

5. Numerical Calculation and Discussion

Upon analyzing the above expressions, we observe that physical Equation (26) is a convergent infinite series function. When n = 10, the calculated results meet the required engineering accuracy. For our analysis, we selected $CoFe_2O_4$ as the material of interest, with a relative material constant of [24]

$$\begin{array}{l} \rho_0 = 5.35 \times 10^3\ \mathrm{kg{\cdot}m^{-2}}, c_{44} = 4.53 \times 10^{10}\ \mathrm{N{\cdot}m^{-2}}, \\ h_{15} = 550\ \mathrm{N{\cdot}A^{-1}{\cdot}m^{-1}},\ \mu_{11} = 5.9 \times 10^{-4}\ \mathrm{N{\cdot}A^{-2}}. \end{array}$$

For our numerical analysis, we consider the incident wave number ka, the incidence angle φ of the SH wave, and the elliptical geometric parameters $e = b/a$ as the characteristic parameters.

Figure 2 illustrates the distribution of the DSCC during the incidence of SH waves along the major axis (φ = 0) and minor axis ($\varphi = \pi/2$) of an elliptical opening with varying geometric parameters (e = 0.3, 0.5, 0.7, 0.9). The symmetric shape of the elliptical opening in the incident direction results in a symmetric distribution of DSCC regions. Moreover, increasing the wave number leads to a decrease in the DSCC, particularly in the shadow region, where the decline is more pronounced. When waves are incident along the major axis of the elliptical opening, the DSCC attains its maximum value as the e value increases. However, the situation is reversed when waves are incident along the minor axis of the elliptical opening. Notably, waves incident from the minor axis exhibit a larger DSCC than those from the major axis.

Figure 3 displays the distribution of the DSCC around the elliptical opening for various wave numbers of SH waves. When e is small, the non-symmetric incidence of SH waves significantly affects the shape of DSCC, as depicted in Figure 3a. As e approaches 1, DSCC becomes symmetrically distributed around the incident direction, and the maximum value decreases. Furthermore, an increase in the incident angle results in an increase in DSCC at low wave numbers.

Figure 4 displays the correlation between the DSCC and the dimensionless wave number. The solid line represents the incidence angle $\varphi = \pi/6$, while the dashed line represents the incidence angle $\varphi = \pi/3$. At the elliptical position $\theta = \pi/2$, the DSCC decreases with an increase in the incidence angle, whereas the opposite trend is observed at θ = 0. The DSCC attenuates with fluctuations in the wave number at both incidence angles. Notably, a lower wave number results in a larger DSCC.

Figure 5 depicts the correlation between the DSCC and the incident angle. The solid line represents a low wave number ka = 0.5, while the dotted line represents a high wave number ka = 3.0. The trend reveals that the DSCC at elliptical positions θ = 0 and $\theta = \pi/2$ changes in opposite directions. In the low-wave-number case, the DSCC curve is monotonically increasing. The DSCC curve is lower than the low-wave-number case for high wave numbers and exhibits fluctuations. Notably, the DSCC change at elliptical position θ = 0 is steeper than at elliptical position $\theta = \pi/2$.

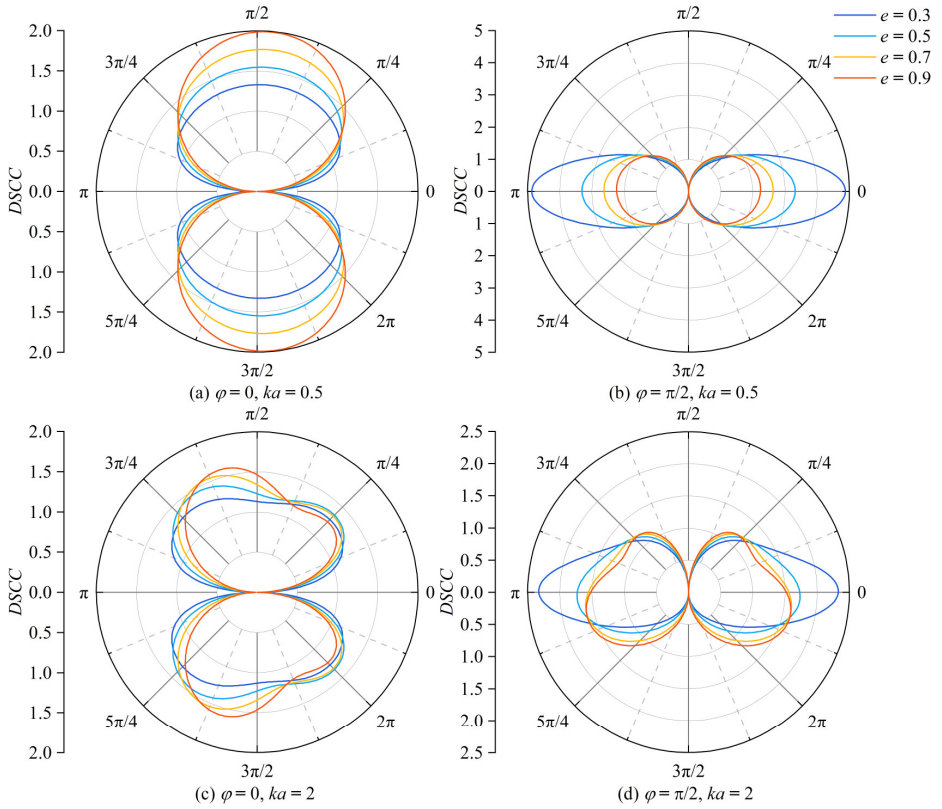


Figure 2. Comparison of distribution of DSCC in elliptical openings under different geometric parameters; incident angle φ, wave number ka and elliptical geometric parameters e.

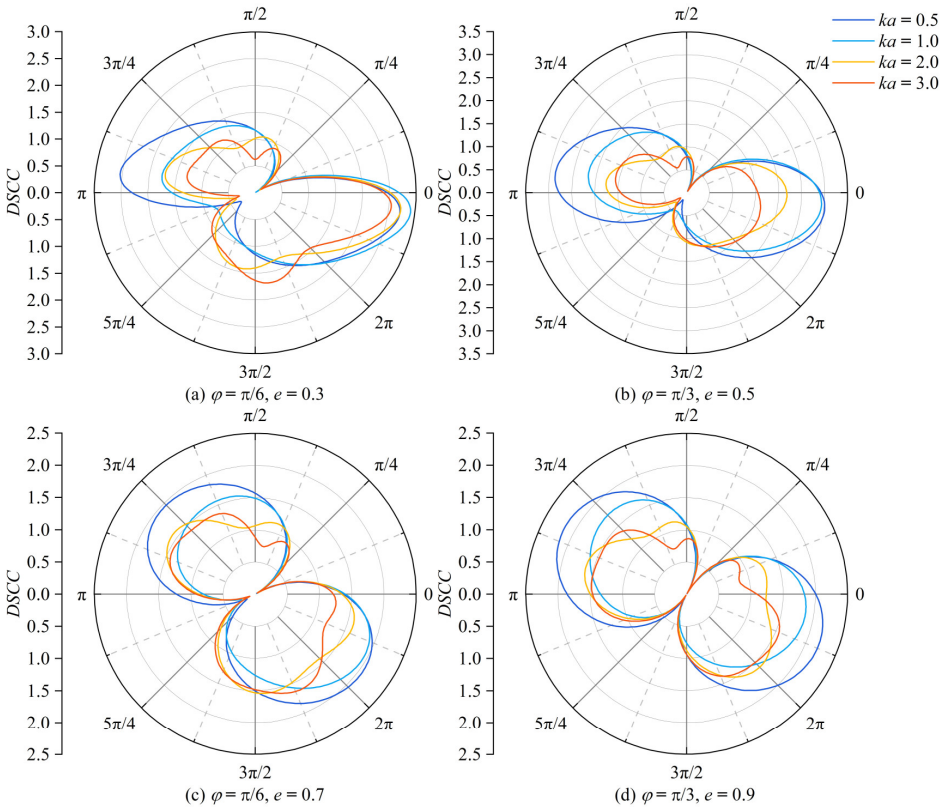


Figure 3. Comparison of distribution of DSCC in elliptical openings under different wave numbers; incident angle φ, wave number ka and elliptical geometric parameters e.

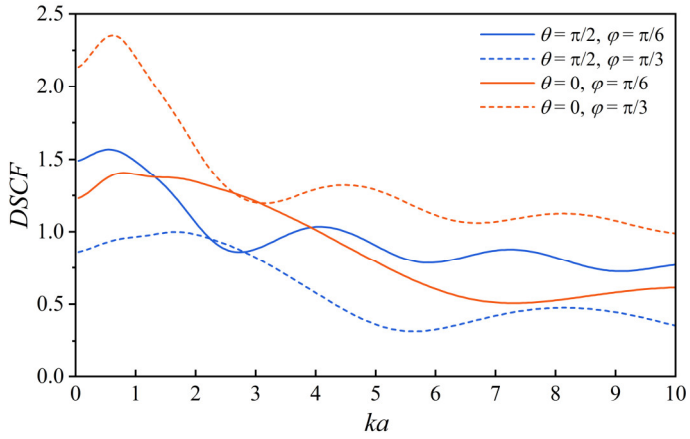


Figure 4. The relationship between DSCC and dimensionless wave number, e = 0.7.

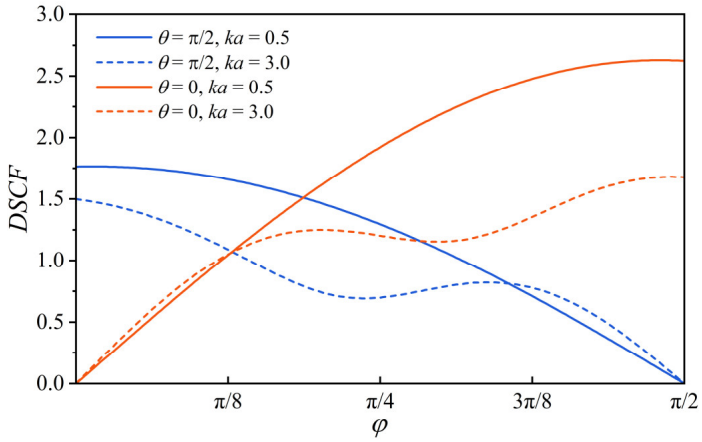


Figure 5. The relationship between DSCC and incidence angle, e = 0.7.

6. Conclusions

This article utilizes complex functions and wave function expansion methods to study the scattering and DSCC issues of steady-state SH waves in piezoelectric materials with non-circular openings. The results show that the shape of the opening, the number of incident waves and the incidence angle have significant effects on the structure. Compared to the theory of elastic media, this method successfully generalizes the mature theory of elastic piezoelectric media to this field, providing a new approach for analyzing the dynamic problems of piezoelectric materials.

Based on the calculation results of a piezomagnetic material structure model with an elliptical opening, the following conclusions can be drawn:

1. The DSCC value around the elliptical opening is related to the illumination region. In the case of incident waves with the same frequency, a larger illumination region will generate a larger DSCC. Therefore, elastic waves traveling along the minor axis of the elliptical opening will cause a larger DSCC than those traveling along the major axis.
2. Elastic waves in the low-frequency range are more significant to consider. In most instances, the DSCC produced by low-frequency waves is higher than that produced by high-frequency waves. Moreover, the DSCC in the illumination region is generally higher than in the shadow region.
3. The DSCC changes differently at different locations in the piezoelectric material with an elliptical opening. The DSCC in specific areas can be much higher than in other places, making them more prone to damage.

Author Contributions: Conceptualization, Z.W. and C.Z.; methodology, J.W.; validation, N.H., R.Z. and Y.G.; formal analysis, W.P.; investigation, J.W. and N.H.; data curation, W.P.; writing—original draft preparation, J.W.; writing—review and editing, Z.W.; supervision, Y.G.; project administration, C.Z.; funding acquisition, N.H. and R.Z. All authors have read and agreed to the published version of the manuscript.

Funding: This research was supported by the Sichuan Science and Technology Program (No. 2022YFG0274).

Institutional Review Board Statement: Not applicable.

Informed Consent Statement: Not applicable.

Data Availability Statement: The authors confirm that the data supporting the findings of this study are available within the article.

Conflicts of Interest: The authors declare no conflict of interest.

Appendix A

The expression of each element in Equation (25) is as follows

$$
\begin{aligned}
&\varepsilon_1 = -\int_0^{2\pi} \mathrm{i}^n J_n(k|\hbar(\zeta)|)\mathrm{e}^{-\mathrm{i}n\varphi}\left\{\frac{\hbar(\zeta)}{|\hbar(\zeta)|}\right\}^n \mathrm{e}^{-\mathrm{i}m\theta}\mathrm{d}\theta,\\
&\varepsilon_2 = -\mathrm{i}^n k\mathrm{e}^{-\mathrm{i}n\varphi}\int_0^{2\pi} J_{n-1}(k|\hbar(\zeta)|)\left\{\frac{\hbar(\zeta)}{|\hbar(\zeta)|}\right\}^{n-1} \hbar'(\zeta)\mathrm{e}^{\mathrm{i}\theta}\mathrm{e}^{-\mathrm{i}m\theta}\mathrm{d}\theta\\
&\qquad -\mathrm{i}^n k\mathrm{e}^{-\mathrm{i}n\varphi}\int_0^{2\pi} J_{n+1}(k|\hbar(\zeta)|)\left\{\frac{\hbar(\zeta)}{|\hbar(\zeta)|}\right\}^{n+1} \overline{\hbar'(\zeta)}\mathrm{e}^{-\mathrm{i}\theta}\mathrm{e}^{-\mathrm{i}m\theta}\mathrm{d}\theta,\\
&F_{1n} = \int_0^{2\pi} H_n^{(1)}(k|\hbar(\zeta)|)\left\{\frac{\hbar(\zeta)}{|\hbar(\zeta)|}\right\}^n \mathrm{e}^{-\mathrm{i}m\theta}\mathrm{d}\theta,\\
&F_{2n} = \int_0^{2\pi} kH_{n-1}^{(1)}(k|\hbar(\zeta)|)\left\{\frac{\hbar(\zeta)}{|\hbar(\zeta)|}\right\}^{n-1} \hbar'(\zeta)\mathrm{e}^{\mathrm{i}\theta}\mathrm{e}^{-\mathrm{i}m\theta}\mathrm{d}\theta\\
&\qquad -\int_0^{2\pi} kH_{n+1}^{(1)}(k|\hbar(\zeta)|)\left\{\frac{\hbar(\zeta)}{|\hbar(\zeta)|}\right\}^{n+1} \overline{\hbar'(\zeta)}\mathrm{e}^{-\mathrm{i}\theta}\mathrm{e}^{-\mathrm{i}m\theta}\mathrm{d}\theta,\\
&I_{1n} = \left(1-\frac{\mu_{11}}{\mu_0}\right)\int_0^{2\pi} \mathrm{e}^{\mathrm{i}n\theta}\mathrm{e}^{-\mathrm{i}m\theta}\mathrm{d}\theta,\ I_{2n} = \left(\frac{2\lambda n}{1+\lambda}\right)\int_0^{2\pi} \mathrm{e}^{\mathrm{i}n\theta}\mathrm{e}^{-\mathrm{i}m\theta}\mathrm{d}\theta,\\
&P_{1n} = \left(1-\frac{\mu_{11}}{\mu_0}\right)\int_0^{2\pi} \mathrm{e}^{-\mathrm{i}n\theta}\mathrm{e}^{-\mathrm{i}m\theta}\mathrm{d}\theta,\ P_{2n} = \left(\frac{2\lambda n}{1+\lambda}\right)\int_0^{2\pi} \mathrm{e}^{-\mathrm{i}n\theta}\mathrm{e}^{-\mathrm{i}m\theta}\mathrm{d}\theta,\\
&Q_1 = -1, Q_2 = 0.
\end{aligned}
\tag{A1}
$$

References

1. Majhi, S.; Pal, P.C.; Kumar, S. Propagation of SH waves in a visco-elastic layer overlying an inhomogeneous isotropic half-space. *Ain Shams Eng. J.* **2018**, *9*, 675–680. [CrossRef]
2. Mondal, S.; Anand, S.S. Propagation of SH waves in corrugated FGPM layer lying over a piezomagnetic half-space. *Mech. Adv. Mater. Struct.* **2019**, *26*, 29–34. [CrossRef]
3. Soh, A.K.; Liu, J.X. Interfacial shear horizontal waves in a piezoelectric-piezomagnetic bi-material. *Philos. Mag. Lett.* **2006**, *86*, 31–35. [CrossRef]
4. Singh, B.M.; Rokne, J. Propagation of SH waves in layered functionally gradient piezoelectric–piezomagnetic structures. *Philos. Mag.* **2013**, *93*, 1690–1700. [CrossRef]
5. Wei, H.-X.; Li, Y.-D.; Xiong, T.; Guan, Y. Propagation of SH waves in a piezoelectric/piezomagnetic plate: Effects of interfacial imperfection couplings and the related physical mechanisms. *Phys. Lett. A* **2016**, *380*, 3013–3021. [CrossRef]
6. Huang, Y.; Li, X.F.; Lee, K.Y. Interfacial shear horizontal (SH) waves propagating in a two-phase piezoelectric/piezomagnetic structure with an imperfect interface. *Philos. Mag. Lett.* **2009**, *89*, 95–103. [CrossRef]
7. Nie, G.; Liu, J.; Fang, X.; An, Z. Shear horizontal (SH) waves propagating in piezoelectric–piezomagnetic bilayer system with an imperfect interface. *Acta Mech.* **2012**, *223*, 1999–2009. [CrossRef]
8. Kuo, H.-Y.; Yu, S.-H. Effect of the imperfect interface on the scattering of SH wave in a piezoelectric cylinder in a piezomagnetic matrix. *Int. J. Eng. Sci.* **2014**, *85*, 186–202. [CrossRef]
9. Sun, W.H.; Ju, G.L.; Pan, J.W.; Li, Y.D. Effects of the imperfect interface and piezoelectric/piezomagnetic stiffening on the SH wave in a multiferroic composite. *Ultrasonics* **2011**, *51*, 831–838. [CrossRef]
10. Qian, Z.; Jin, F.; Wang, Z.; Kishimoto, K. Dispersion relations for SH-wave propagation in periodic piezoelectric composite layered structures. *Int. J. Eng. Sci.* **2004**, *42*, 673–689. [CrossRef]

11. Wang, J.H.; Zhou, X.L.; Lu, J.F. Dynamic stress concentration around elliptic cavities in saturated poroelastic soil under harmonic plane waves. *Int. J. Solids Struct.* **2005**, *42*, 4295–4310. [CrossRef]
12. Li, J.X.; Liu, X.G.; Zhao, Y.B. Green's functions for anisotropic magnetoelectroelastic solids with an elliptical cavity or a crack. *Int. J. Eng. Sci.* **2001**, *39*, 1405–1418. [CrossRef]
13. Pan, E.; Heyliger, P.R. Exact solutions for magneto-electro-elastic laminates in cylindrical bending. *Int. J. Solids Struct.* **2003**, *40*, 6859–6876. [CrossRef]
14. Pan, E.; Han, F. Exact solution for functionally graded and layered magneto-electro-elastic plates. *Int. J. Eng. Sci.* **2005**, *43*, 321–339. [CrossRef]
15. Pang, Y.; Liu, Y.S.; Liu, J.X.; Feng, W.J. Propagation of SH waves in an infinite/semi-infinite piezoelectric/piezomagnetic periodically layered structure. *Ultrasonics* **2016**, *67*, 120–128. [CrossRef]
16. Ezzin, H.; Amor, M.B.; Ghozlen, M.H.B. Propagation behavior of SH waves in layered piezoelectric/piezomagnetic plates. *Acta Mech.* **2016**, *228*, 1071–1081. [CrossRef]
17. Nobili, A.; Radi, E.; Vellender, A. Diffraction of antiplane shear waves and stress concentration in a cracked couple stress elastic material with micro inertia. *J. Mech. Phys. Solids* **2019**, *124*, 663–680. [CrossRef]
18. Wang, Y.-Z.; Li, F.-M.; Huang, W.-H.; Jiang, X.; Wang, Y.-S.; Kishimoto, K. Wave band gaps in two-dimensional piezoelectric/piezomagnetic phononic crystals. *Int. J. Solids Struct.* **2008**, *45*, 4203–4210. [CrossRef]
19. Yu, J.G.; Lefebvre, J.E.; Zhang, C. Guided wave in multilayered piezoelectric–piezomagnetic bars with rectangular cross-sections. *Compos. Struct.* **2014**, *116*, 336–345. [CrossRef]
20. Cao, X.; Shi, J.; Jin, F. Lamb wave propagation in the functionally graded piezoelectric–piezomagnetic material plate. *Acta Mech.* **2012**, *223*, 1081–1091. [CrossRef]
21. Pang, Y.; Liu, J.; Wang, Y.; Fang, D. Wave propagation in piezoelectric/piezomagnetic layered periodic composites. *Acta Mech. Solida Sin.* **2008**, *21*, 483–490. [CrossRef]
22. Li, L.; Wei, P.J. The piezoelectric and piezomagnetic effect on the surface wave velocity of magneto-electro-elastic solids. *J. Sound Vib.* **2014**, *333*, 2312–2326. [CrossRef]
23. Zakharenko, A.A. A study of SH-SAW propagation in cubic piezomagnetics for utilization in smart materials. *Waves Random Complex Medium* **2012**, *22*, 488–504. [CrossRef]
24. Zhong, Y.F.; Chen, L.; Yu, W.B.; Zhang, L.L. Asymptotical construction of a fully coupled, Reissner–Mindlin model for piezoelectric and piezomagnetic laminates. *Compos. Struct.* **2012**, *94*, 3583–3591. [CrossRef]

Disclaimer/Publisher's Note: The statements, opinions and data contained in all publications are solely those of the individual author(s) and contributor(s) and not of MDPI and/or the editor(s). MDPI and/or the editor(s) disclaim responsibility for any injury to people or property resulting from any ideas, methods, instructions or products referred to in the content.